FIELD DISTRIBUTIONS IN THE TRAPPED IMAGE GUIDE

W. B. Zhou and T. Itoh
Dept. of Electrical Engineering
The University of Texas at Austin
Austin, Texas 78712

Abstract

An efficient analytical method based on Weber-Schafheitlin integral is presented for accurate field calculation in the trapped image guide. Several numerical results of the field distributions are presented and compared with measured data at Ku-band.

Introduction

The trapped image guide (Fig. 1) has been proposed for reducing the radiation loss at bends in dielectric millimeter-wave integrated circuits.[1] It has also been used for a leaky wave antenna.[2] An efficient method based on the effective dielectric constants and surface impedance has been developed for dispersion characteristics of this waveguide.[3] Although the dispersion characteristics so derived agree well with experimental data, the predicted field distribution can correlate with measured results only qualitatively. It is widely recognized that more accurate analyses are required for the field distributions than for the dispersion in a class of open dielectric waveguides.[4]

In this paper, we present a method based on Weber-Schafheitlin discontinuity integral for deriving an accurate field distribution in the trapped image guide. Such knowledge is indispensable when millimeter-wave components such as leaky wave antennas and directional couplers are designed. One of the advantages is that in this method the boundary condition on the ground plane $y = 0$, $|x| > a + c$ is automatically satisfied.

Method of Analysis

In this paper, we will discuss only E^y_{pq} modes. Our main interest is the field distributions for the region $y \geq 0$, because these are the ones important for component design. In addition, they are more difficult to describe than those in the trough region where the field is confined within $|x| < a + c$.

For region $y < 0$, we use the effective dielectric constant method to obtain a hypothetical medium ε_e filling the trough. First, we obtain the hypothetical value ε_{el} in Fig. 1(b) by a now conventional EDC method.[1] ε_e is obtained next such that the phase velocities of trough lines (those with infinitely high side walls) filled with ε_e and ε_{el} are identical.[3] In [3], the propagation constant β of the original structure Fig. 1(a) is derived from Fig. 1(c) by matching the surface impedances at $y = 0$ looking upward and downward.

We will use the values of β so derived in the derivation of the field distribution in this paper. For $y < 0$, we expand the field in a sinusoidal series appropriate for Fig. 1(c). For instance,

$$E_y = \sum_{n=1}^{\infty} A_n \sin\left[\frac{n\pi}{2(a+c)}\right](a + c - x) \cos[h_n(y + b)] \qquad (1)$$

$$h_n = \left\{\varepsilon_e k_o^2 - \beta^2 - \left[\frac{n\pi}{2(a+c)}\right]^2\right\}^{1/2} \qquad (2)$$

Obviously, this representation is not accurate enough. However, we simply use this expansion to obtain accurate information of the field in $y \geq 0$ which is our main interest as shown below.

In the semi-infinite region $y \geq 0$, we expand E_y as

$$E_y = \sum_{m=0}^{\infty} [C_m Y_m^-(x,y) + D_m Y_m^+(x,y)] \qquad (3)$$

where

$$Y_m^-(x,y) = \sqrt{x} \int_0^\infty \frac{J_{-\frac{1}{2}}(k_x x)\, J_{2m+1}(k_x(a+c))}{\sqrt{k_x}\sqrt{k_x^2 + \beta^2 - k_o^2}} \exp\left(-y\sqrt{k_x^2 + \beta^2 - k_o^2}\right) dk_x$$

$$Y_m^+(x,y) = \sqrt{x} \int_0^\infty \frac{J_{+\frac{1}{2}}(k_x x)\, J_{2m+2}(k_x(a+c))}{\sqrt{k_x}\sqrt{k_x^2 + \beta^2 - k_o^2}} \exp\left(-y\sqrt{k_x^2 + \beta^2 - k_o^2}\right) dk_x$$

$J_\nu(x)$: Bessel function

Note that $\sqrt{x}\, J_{\pm\frac{1}{2}}(k_x x)$ are sinusoidal functions and hence $Y_m^\pm$ satisfy the Helmholtz equation. These rather complex forms of expansion are chosen with a good reason. Notice that E_x and E_z are proportional to $\partial E_y/\partial y$, which is in turn proportional to

$$\int_0^\infty \frac{J_{\pm\frac{1}{2}}(k_x x)\, J_\nu(k_x(a+c))}{\sqrt{k_x}} \exp\left(-y\sqrt{k_x^2 + \beta^2 - k_0^2}\right) dk_x$$

($\nu = 2m + 1$ or $2m + 2$). For $y = 0$, the above quantity becomes the one called Weber-Schafheitlin integral[5] and becomes identically zero for $|x| > a + c$. Therefore, choice of $Y_m^\pm(x,y)$ satisfies the boundary conditions on E_x and E_z automatically.

We now impose the interface matching conditions at $y = 0$, $|x| < a + c$ on the tangential fields from (1) and (3). After some mathematical manipulations, we obtain a matrix equation for A_n, C_m and D_m. Although the matrix elements contain infinite integrals of the form $\int_0^\infty \frac{J_m(\xi)\, J_n(\xi)}{\xi^2} d\xi$, they can be evaluated efficiently as the integrand decreases quickly. Solving this equation for these coefficients, we can find the field distributions.

0149-645X/83/0000-0187 $01.00 © 1983 IEEE

Numerical Results and Experimental Verification

We consider here only the dominant E^y_{11} mode in the channel region. The normalized distributions of the field components E_y and E_z outside of the channel are presented in Fig. 2(a) and (b), respectively. It is seen that the boundary condition $E_z = 0$ at $y = 0$, $|x| > a + c$ is satisfied in the numerical results.

We performed measurements of the field distribution of E_y outside of the channel by means of a movable probe at 14 GHz. Comparison between the numerical results and the experimental data is given in Fig. 3. It is evident that agreement between theoretical and experimental results is quite good.

Fig. 4 presents relative decay as a function of distance above the $y = 0$ plane in the symmetry plane $x = 0$.

Fig. 5(a) and 5(b) illustrate the x-variation of the field components E_y and E_z at different frequencies. It is evident that more fields are concentrated in the central area when the frequency is increased. Fig. 6 presents the variation of the relative strength of the field components $E_y(0,0)$ and $E_z(0,0)$ with respect to frequency. It is clear that the contribution of the axial component E_z increases with frequency.

Conclusion

In this paper, we have presented a method based on the Weber-Schafheitlin integral and the EDC method for predicting the field profile above the channel in the trapped image guide. Some numerical results are presented. Experimental verification of the field profile predicted by this method is included. This method can be applied to other open waveguides with a similar configuration.

Acknowledgment

This work was in part supported by U.S. Army Research Office Contract DAAG29-81-K-0053.

References

(1) T. Itoh and B. Adelseck, "Trapped image guide for millimeter-wave circuits," IEEE Trans. Microwave Theory and Tech., Vol. MTT-28, No. 12, pp. 1433-1436, December 1980.

(2) T. Itoh and B. Adelseck, "Trapped image leaky-wave antennas for millimeter wave applications," IEEE Trans. Antennas and Propagation, Vol. AP-30, No. 3, pp. 505-509, May 1982.

(3) W. B. Zhou and T. Itoh, "Analysis of Trapped image guides using effective dielectric constants and surface impedances," 1982 IEEE MTT International Microwave Symposium, Dallas, TX, June 1982

(4) S. T. Peng and A. A. Oliner, "Guidance and leakage of a class of open dielectric waveguides," IEEE Trans. Microwave Theory and Techniques, Vol. MTT-29, No. 9, pp. 843-855, September 1981.

(5) K. Hongo, Y. Ogawa, T. Itoh and K. Ogusu, "Field distribution in a flanged parallel-plate waveguide," IEEE Trans. Microwave Theory and Tech., Vol. MTT-23, pp. 538-560, July 1975.

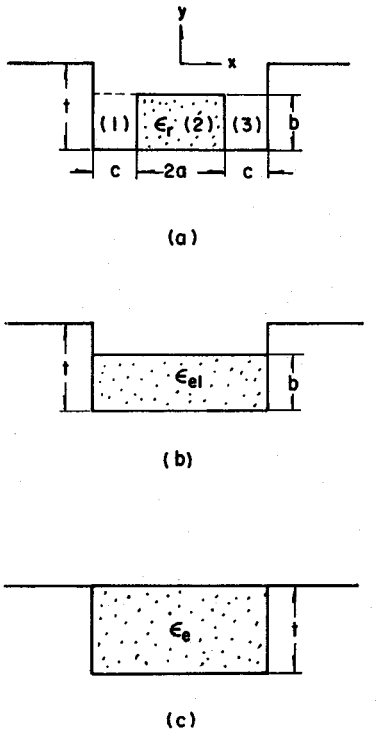

Fig. 1 Analysis models of trapped image guide

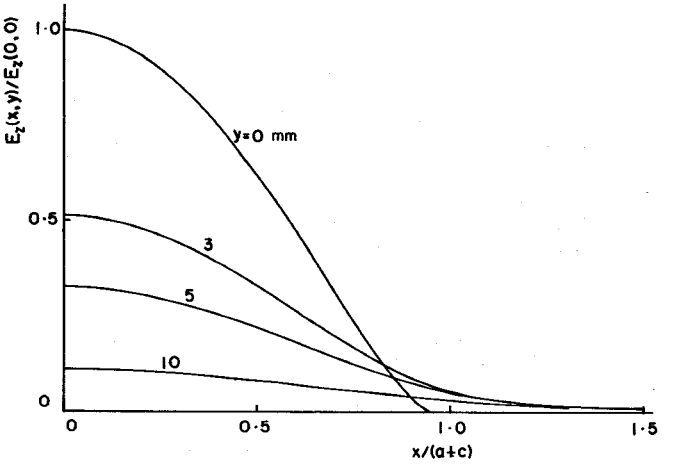

Fig. 2 Normalized distribution of field component E_z

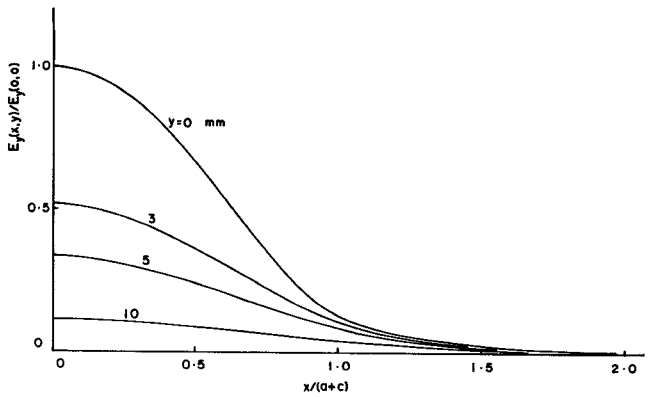

Fig. 2b Normalized distribution of field component E_y.

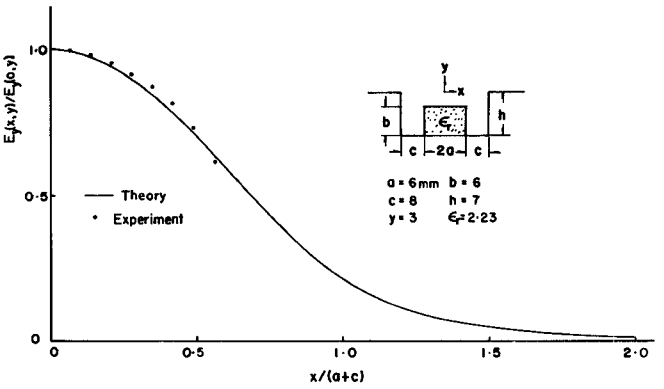

Fig. 3 Comparison between theoretical and experimental values of E_y.

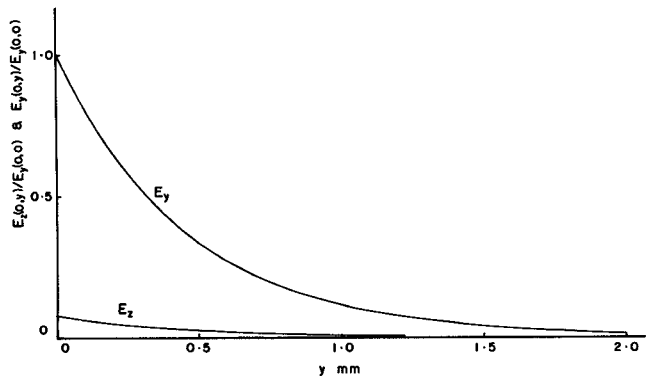

Fig. 4 Normalized E_z and E_y distributions vs. Y.

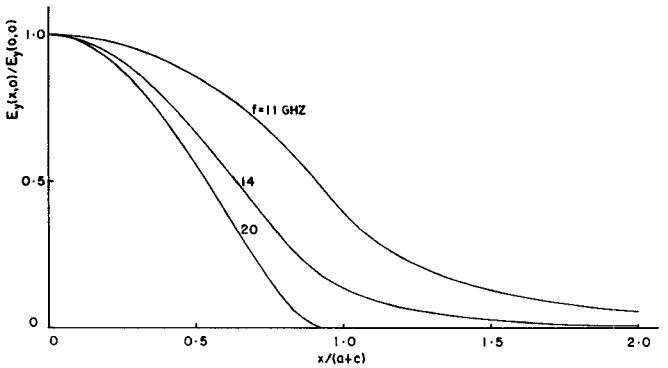

Fig. 5a Normalized distribution of field component E_y at different frequencies.

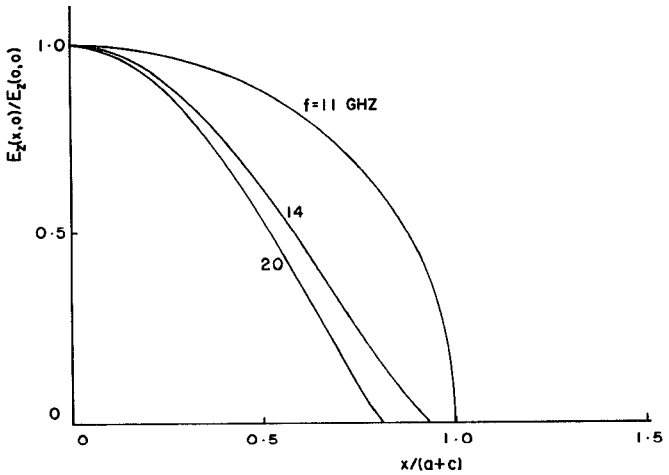

Fig. 5b Normalized distribution of field component E_z at different frequencies.

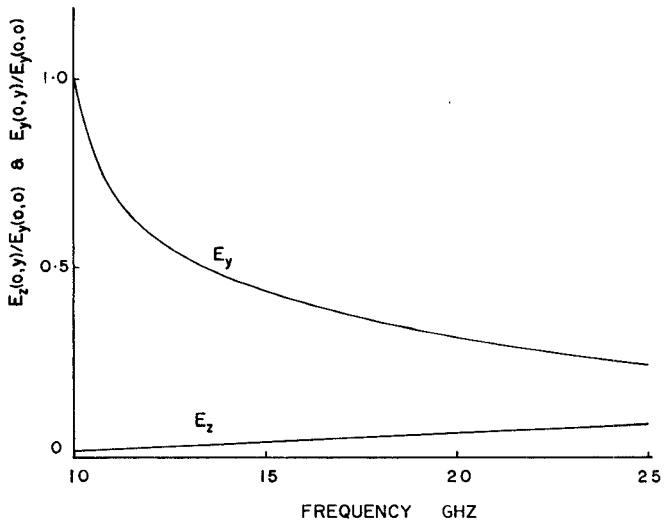

Fig. 6 Relative field strength at (o,y) vs. frequency.